Chapter 3

Measurement and Characterization Tools

3.1. General Description of Synthesis Apparatus

Mainly liquid phase exfoliation and hydrothermal process were used for the synthesis of the 2-D nanomaterials discussed in this thesis. Following section contain the brief description of these processes. For chemical synthesis of $VOPO_4$, $2H_2O$ nanosheets reflux method was used.

3.1.1. Ultra-Sonicator

A horn (high power) sonicator and bath sonicator was used for the liquid phase exfoliation of transition metal oxides (TMOs) from their bulks. Low power bath sonicator was also used for exfoliation of graphene, CNTs and other materials prepared by hydrothermal process for the thin films preparation. Due to the large ultrasonic energy, solvent molecules are oscillates about their mean position at the high frequency (~ 20 kHz). The shock waves associated with this high frequency oscillation generates large local shear stresses, which breaks the van der Waals bounds of the layered materials. An ultrasonic cleaner was used to clean the substrates (glass, quartz, Si, etc.) using distilled water and preparation of grid required for the HRTEM study. In our lab we have a number of ultra-sonicator as shown in the fig 3.1 with an additional heating arrangement.

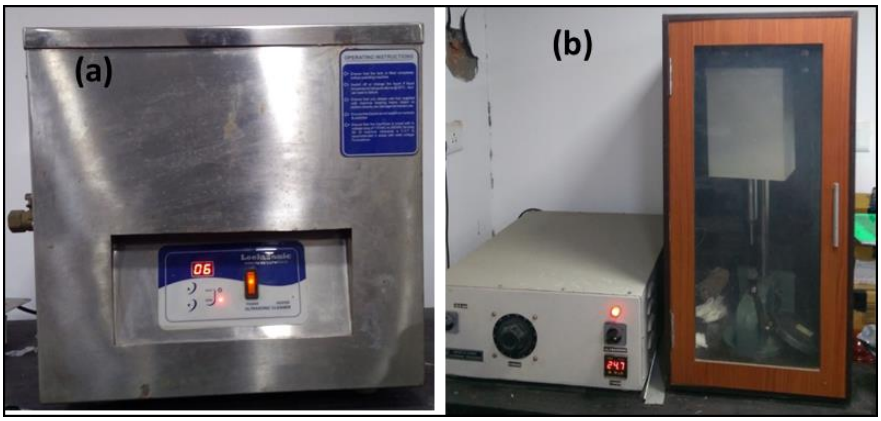

Figure.3.1 Photograph of bath-ultrasonicator(a), Horn-sonicator(b)

3.1.2. Oven and Autoclave

An oven was used for the purpose of performing any hydrothermal reaction. The range of the furnace was up to $500^{O}C$ and the heating rate can be controlled by an electronic temperature controller with an accuracy of ± 0.2 ^{O}C. The photograph of the used furnace is shown in the Fig. 3.2(a). Hydrothermal synthesis was done using autoclave equipment. An autoclave is a pressurized vessel to heat aqueous solution above their boiling point at a pressure higher than normal pressure. It is basically a cylindrical iron chamber fitted with an iron screw cap. The cap may be fitted very tightly with the iron

chamber so that it can withstand a very high pressure during reaction. Synthesis of BiOCl and MoS_2 nanosheets through hydrothermal process were done with an autoclave arrangement as shown in Fig. 3.2(b) and (c).

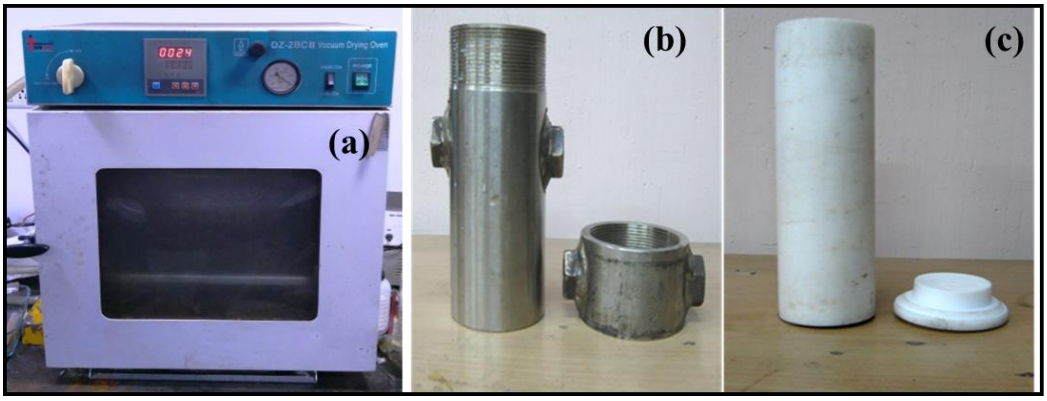

Figure.3.2 *Digital photograph box-furnace and oven (a), Photographs of autoclave jacket (b) and teflon used inside an autoclave(c)*

3.2. Supporting Accessories

The supporting accessories that have been used in the working periods are the following:

3.2.1. Magnetic Stirrer and Centrifuge

The magnetic stirrer is a very essential supporting apparatus for chemical synthesis. It can stir a magnetic piddle inside the solution of the beaker through a revolving magnetic setup attached with it. The stirrer can also heat the solution at a desired temperature using heater arrangement associated with it as shown in Fig.3.3(a). The hot plate of the stirrer can also use to thin films transfer on different substrates.

Centrifuge is mainly used to separate impurities from the synthesized products. The rotational speed of the centrifuge can be set up to 18,000 rpm. The photograph of the centrifuge is shown in Fig. 3.3.(b) The synthesis and functionalization of all the carbon structures as well as the synthesis of Mn_3O_4 nanorods were very much associated with the proper utilization of magnetic stirrer, ultra-sonicator and centrifuge.

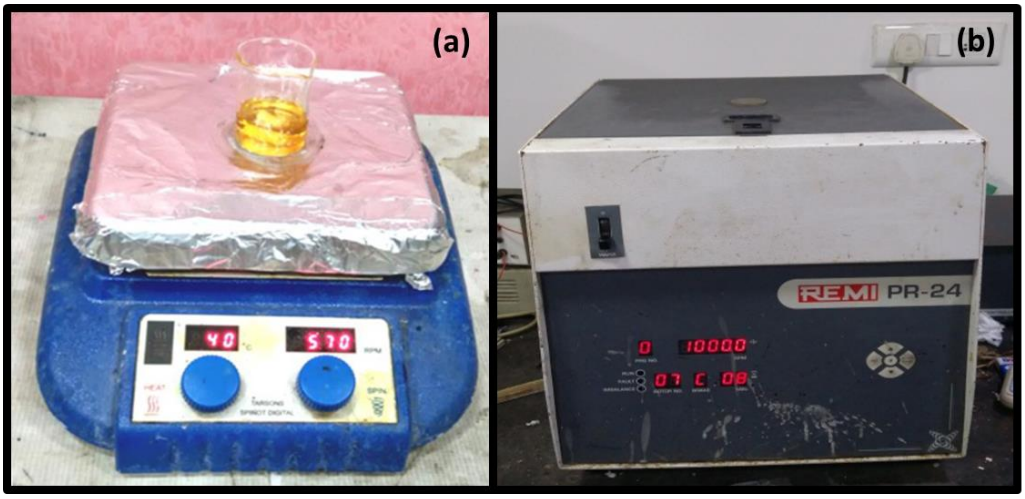

Figure.3.3 Photographs of the (a) magnetic stirrer and (b) Centrifuge.

3.3. Principle and Description of Characterizing Instruments

To characterize the samples several sophisticate instruments were used. A brief description of all those instruments and their working principal are given in the following section.

3.3.1 X-Ray Diffractometer (XRD)

The structural properties of the prepared materials can investigate by well-known X-ray diffraction method. This technique has been applied to stress and strain measurement, chemical phase analysis, the study of phase equilibrium, measurement of particle size, as well as to determine crystal structure. A Rigaku-Ultima III X-ray diffractometer with CuKα radiation (λ = 1.5418 Å) was used for characterization of the synthesized samples. When a highly collimated beam of X-rays fall on a material, due to the diffraction from the crystalline phases of the sample a diffraction pattern is observe. To determine the materials and its structural properties, the obtained diffraction patterned is used. One can easily found the lattice spacing from this diffraction pattern using 1^{st} order Bragg's equation.

$$\lambda = 2d \sin\theta$$

Where λ = wavelength of electron,

d = Interplanar spacing and

θ = glancing angle.

In terms of the angle of diffraction 2θ and orientation of the sample, diffracted X-rays intensity is measured. Fig.3.4 shows schematic diagram of the X-Ray Diffractometer (XRD).

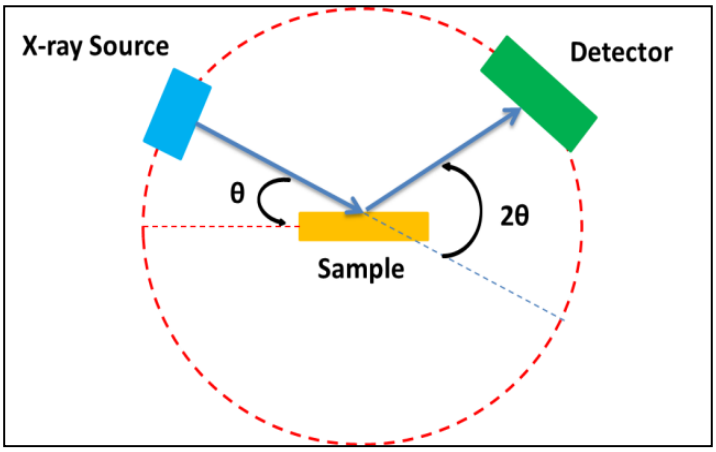

Figure.3.4 Schematic diagram of the X-Ray Diffractometer (XRD)

3.3.2. Ultraviolet-visible-near infrared (UV-Vis-NIR) spectrophotometer

UV-Vis spectroscopy (Lambda-950 spectrometer, Perkin Elmer, USA) spectrophotometer was used to measure the extent to which the sample absorb or transmit the light of varying wavelength. The wavelength could be varied from 200 to 3500 nm. Also reflectance globe was attached to the instrument for recording the reflectance of the sample. Figure 3.5 shows Block diagram of UV-Vis-NIR spectrophotometer.

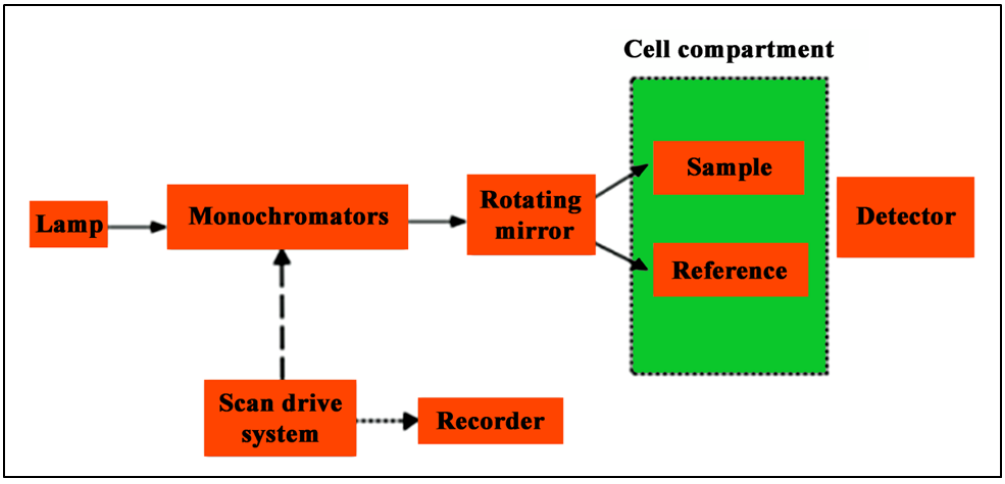

Figure.3.5 Schematic diagram of the Ultraviolet-visible-near infrared (UV-Vis-NIR) spectrophotometer

3.3.3. X-ray photoelectron spectrometer

X-ray photoelectron spectroscopy (ULVAC-PHI5000 Versa Probe II spectrometer) with A1 Kα radiation source of photon energy 1486.6 eV was used to examine the composition of the material of samples and chemical state of the dopants of the sample.

Fig.3.6 represent the schematically diagram of (mechanism) electron emission from metal surface. X-ray of known energy falls on a material due to which photoemission of electron from the sample takes place. Relation between kinetic energy (E_k) of the emitted electron and the binding energy (E_b) is $E_b=h\nu-E_k$, where hν is the energy of incident X-Ray, which can be measured as a function of number of electrons through the instrument. Every element has its own set of binding energies because of that unique property; XPS can be used to recognize the surface element of the samples. The concentration of the elements can also be determined by the Peak areas at nominal binding energies.

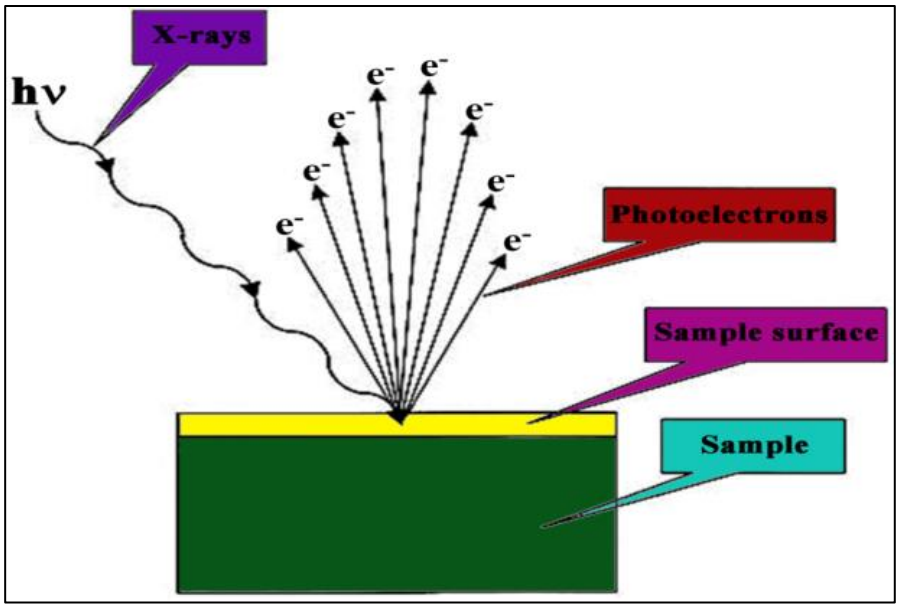

Figure.3.6 Schematic diagram of the X-ray photoelectron spectrometer.

3.3.5 Field Emission Scanning Electron Microscope (FESEM)

Field emission scanning electron microscope (FESEM) images were taken by a FEI; MERLIN (Carl Zeiss) and SUPRA40 field emission scanning electron microscope.Surface morphology of the samples was determined by FESEM images. The resolution of the instrument was 3 nm. The accelerating voltage is lying in the range between 1.5 to 30 kV, in 55 steps. The magnification could be varied 12 to 10^6 X. Probe-current range was 4 pA -10 nA. The schematic diagram of the scanning electron microscope is shown in Fig.3.7

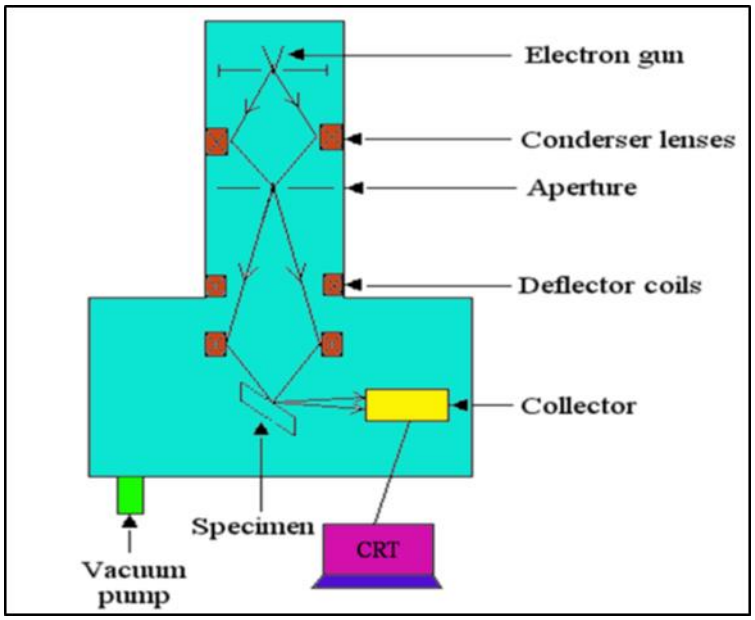

Figure.3.7 Schematic diagram of the Scanning Electron Microscope (SEM) and Field Emission Scanning.

3.3.4. High-resolution Transmission Electron Microscope (HRTEM)

A beam of electrons is spread through several apertures and lenses in the HRTEM setup. The image is focused on a phosphor screen after passed the beams through the samples. The beam may pass through the sample because the electron beam is much more energetic than the beam used in SEM (150-250 kV in HRTEM compared to 1.5-30 kV in FESEM). So, the samples with lesser thickness (< 100 nm) can give good quality images in HRTEM than in SEM. The advantages of HRTEM are high resolution, easy particle size measurement and the ability to determine crystallinity easily. This means that very small crystals can be identified and their crystal structures can be determined easily. A useful crystallographic data can also be obtained from selected area electron diffraction pattern. A schematic diagram of HRTEM is shown in Fig.3.8. In this work a transmission electron microscope (JEM 2100, at an accelerating voltage of 200 keV) was used to study the microstructure of the various samples.

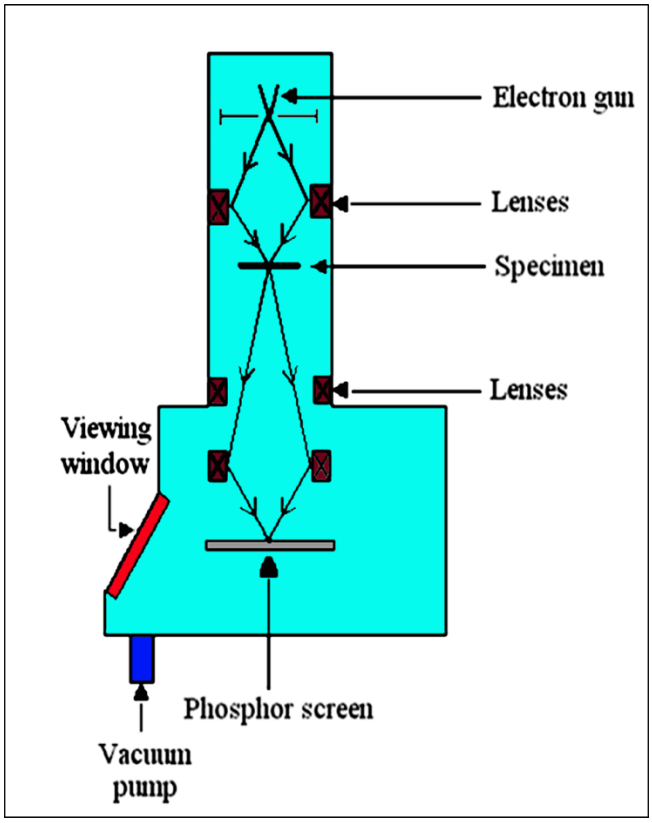

Figure.3.8 Schematic diagram of the High-resolution Transmission Electron Microscope (HRTEM)

3.3.5. Atomic Force Microscope (AFM)

Atomic Force Microscopy (VEECO di CP-II AFM), was used to study the morphology of the thin films. Due to superior resolution, the AFM has some advantages over (SEM). The AFM provides direct height measurements, extraordinary topographic contrast, and unobscured views of surface features. In addition there is no coating required for AFM measurements.

In AFM without expensive sample preparation, 3-dimensional AFM images are obtained and more complete information than the 2-dimensional profiles available from cross-sectioned samples. In general the force acting between the cantilever and the sample is a sum of Vander Waals, electrostatic, magnetic, electro-dynamic and capillary forces, which are compensated by elasticity forces resulting from the cantilever bending and the sample deformation. Cantilevers are normally 100 to 350 microns long, 0.3 to 2 microns thick and their width is about 40 microns. Thick and short cantilevers, as a rule, have high spring constant and differ in higher resonant frequencies. The cantilevers spring constants are within the range from 10^{-2} up to 10^{2} N/m. This allows using

appropriate probes both for soft samples study, for example, biological objects, and for performing the AFM lithography (nano scratching).A simple schematic diagram of the AFM is shown in the Figure 3.9.

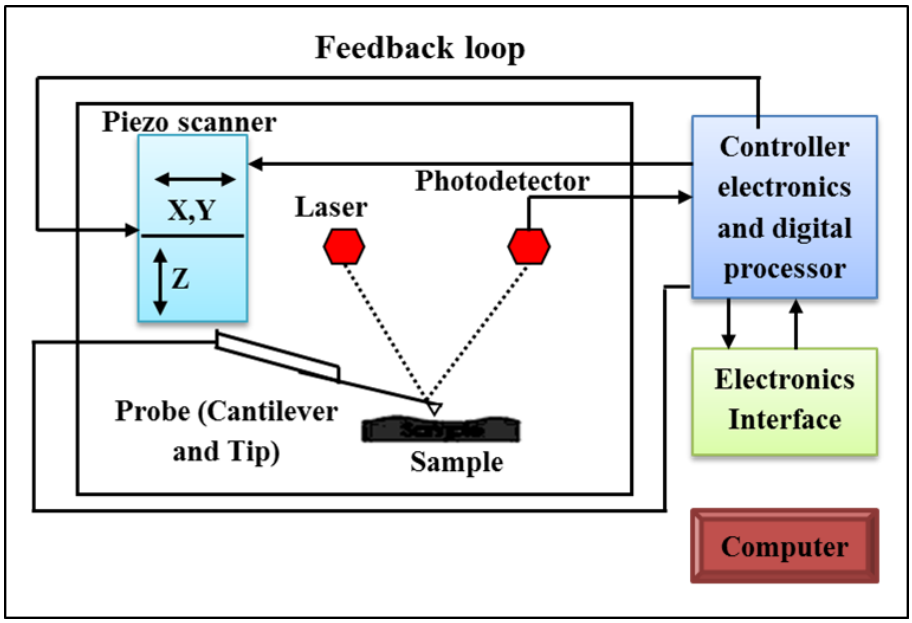

Figure.3.9 Schematic diagram of the Atomic Force Microscope (AFM)

3.3.6. Raman spectroscopy

To study the vibrational properties of the nanostructured material, Raman spectroscopy is one of the useful tools. From the Raman Spectroscopy, the information about structure, phase, phonon confinement, grain size etc. can be determined. When a monochromatic radiation is scattered by molecules, a small fraction of the scattered radiation is observed to have a different frequency from the incident one due to the inelastic scattering. This down converted frequency shift is known as Strokes shifted scattering. Whereas, when the incident radiation absorbs a phonon and emerges with higher energy Anti-strokes shift scattering occurs. A stroke mode scattering is usually monitored because Anti-strokes mode is weaker than the Stroked mode.In Raman Spectroscopy, an intense monochromatic radiation, i.e., a laser source is incident on the sample. The weak scattered light is passed through the monochromator to reject the Raleigh scattering and Photodetector detect the Raman shifted wavelength. The phonon confinement in a material can be observed as the shift in the Raman line frequencies from the bulk material. Acoustic modes of bulk materials are not observable because of their low frequencies but in case of nanostructured material it appears in the measurable

range. The frequency of the acoustic mode is inversely proportional to the size of the particles. Confinement of optical phonon results in the frequency shift and asymmetrical broadening of longitudinal (LO) and transverse optical (TO) mode line shape. In the present work, Raman spectra were obtained with Raman spectroscopy (IHR550 and the laser of excitation wavelength 532 nm).The picture of the block diagram of the optical instrument is shown in Fig. 3.10.

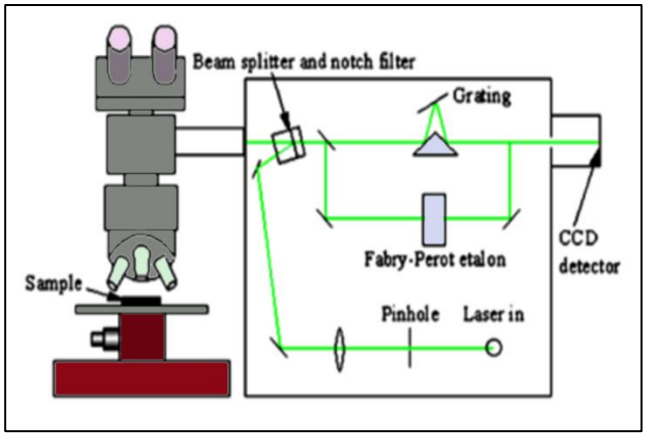

Figure.3.10 Schematic diagram of the Raman spectroscopy

3.4 Experimental techniques for studying electrochemical performances of supercapacitors

In the present study we have done cyclic voltammetry, galvanometric charging discharging and electrochemical impedance spectroscopy to investigate the performance of supercapacitors using CHI 600E Series Electrochemical Analyzer/Workstation as shown in the fig 3.11.

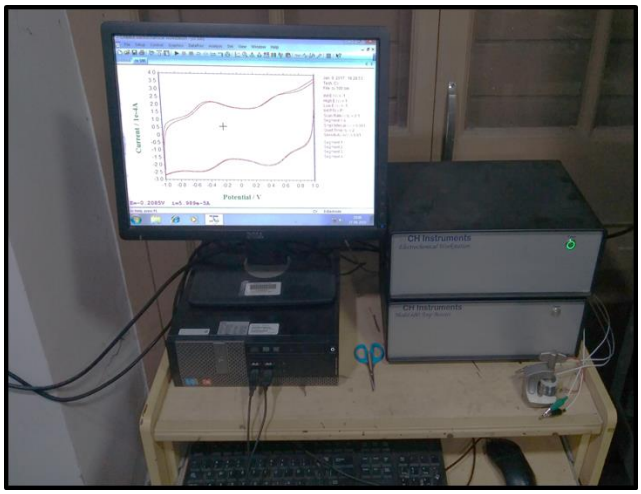

Figure.3.11 CHI 600E Series Electrochemical Analyzer/Workstation.

A brief description of the methods employed is given below:

(a) Cyclic voltammetry:

Cyclic voltammetry is a well-known technique to study the electrochemical performance of supercapacitors, in which a potential is applied to the working electrodes at a constant rate and current flowing through the electrode is measured over a specified potential window. EDLCs shows rectangular shaped CV curves whereas PSCs shows redox peaks in their CV curves.

The specific capacitance of the two electrode symmetric and asymmetric supercapacitors can be calculated from the CV curves using equations (1) and (2) respectively, where m is the total mass of the electrode materials, ν (V/s) is the scan rate and ΔV represent potential window. Energy density (E) and power density (P) can also be calculated from the equations (3) and (4) for symmetric supercapacitor and that for asymmetric supercapacitor from equations (5) and (6).[1-3]

$$C_{symmetric} = \frac{4 \int \mathrm{I}_1 \, \mathrm{dV}}{\nu \mathrm{m} \Delta \mathrm{V}} \ldots\ldots\ldots\ldots\ldots (1)$$

$$C_{asymmetric} = \frac{2 \int \mathrm{I}_1 \, \mathrm{dV}}{\nu \mathrm{m} \Delta \mathrm{V}} \ldots\ldots\ldots\ldots\ldots (2)$$

$$E_{symmetric} = \frac{1}{8} C(\Delta V)^2 \ldots\ldots\ldots \quad (3)$$

$$P_{symmetric} = \tfrac{1}{8} C \, \Delta V \nu \quad \ldots\ldots\ldots\ldots (4)$$

$$E_{asymmetric} = \frac{1}{4} C(\Delta V)^2 \ldots\ldots\ldots \quad (5)$$

$$P_{asymmetric} = \tfrac{1}{4} C \, \Delta V \nu \quad \ldots\ldots\ldots\ldots (6)$$

(b) Galvanometric charging discharging (GCD):

In GCD measurements a constant current density is applied between the electrodes until the lower or higher potential is reached. We can also calculate the specific capacitances from the GCD curves according to the equations (7) and (8) for symmetric and asymmetric two electrode supercapacitors respectively, where m is the total mass of the electrode materials, I is the applied current and $\Delta \mathrm{V}/\Delta \mathrm{t}$ represent slope of the discharge curves after IR drop. [45] The internal resistance of the supercapacitors can also be calculated from the very short IR drop, which is obtained in the initial portion of the discharge curves. For EDLC rest of the discharge curve after IR drop is linear and that for PSCs and HSCs large deviations in linearity occurs.

$$C_{symmetric} = \frac{4I\,\Delta t}{m\,\Delta V} \ldots\ldots\ldots\ldots\ldots\ldots (7)$$

$$C_{asymmetric} = \frac{2I\,\Delta t}{m\Delta V} \ldots\ldots\ldots\ldots\ldots\ldots (8)$$

(c) Electrochemical impedance spectroscopy (EIS):

Kinetic parameters of the electrochemical processes such as charge transfer, ion diffusion can easily determine by the electrochemical impedance spectroscopy technique, where the impedance data are recorded at the open circuit voltage by applying a small alternating voltage ($\pm$ 5mV to $\pm$10 mV) over a frequency window (1mHz to 1MHz).The series resistance (R_s) and charge transfer resistance (R_{ct}) can be calculated from the EIS graph (Nyquist plot).The diameter of the semicircle in the medium frequency region represent the value of R_{ct}, Low value of R_{ct} indicates fast electrochemical reactions. An inclined line a in the low frequency region displays Warburg impedance. From the linear part of the Bode plot (log |Z| vs. log n curve) capacitance value can also be calculated from the equation (9), where |Z| and n represent the imaginary part of impedance and frequency respectively. [4] The Bode plots show that capacitance value decreases with the increasing frequency because at high frequency electrolyte ions cannot penetrate into the microspores.

$$C = \frac{1}{2\pi f|Z|} \ldots\ldots\ldots\ldots\ldots\ldots (9)$$

3.5 References

1. C. Wu, X. Lu, L. Peng, K. Xu, X. Peng, J. Huang, G. Yu and Y. Xie, Nat.Commun., 2013, 4, 2431.
2. H. Wang, H. Yi, X Chen and X. Wang, J. Mater. Chem. A 2014, 2, 3223-3230.
3. S. Ratha and C. S. Rout. RSC Adv. 2015, 5, 86551-86557.
4. P. Taberna, P. Simon and J.F. Fauvarque, Journal of the Electrochemical Society, 2003, 150, A292-A300.